This is the accepted manuscript made available via CHORUS. The article has been published as:

# Low-energy structure of above-threshold-ionization electron spectra: Role of the Coulomb threshold effect

Dmitry A. Telnov and Shih-I Chu (□□□)

Phys. Rev. A **83**, 063406 — Published 10 June 2011

DOI: 10.1103/PhysRevA.83.063406

# Low-Energy Structure of ATI Electron Spectra: Role of Coulomb Threshold Effect

Dmitry A. Telnov[1,*] and Shih-I Chu (朱時宜)[2,3,†]

[1] *Department of Physics, St. Petersburg State University, 198504 St.Petersburg, Russia*
[2] *Department of Chemistry, University of Kansas, Lawrence, Kansas 66045*
[3] *Center for Quantum Science and Engineering, Department of Physics, National Taiwan University, Taipei 10617, Taiwan*

Recent experimental observations of above-threshold ionization of rare gas atoms and diatomic molecules by mid-infrared laser fields [C. I. Blaga *et al.*, Nature Phys. **5**, 335 (2009); W. Quan *et al.*, Phys. Rev. Lett. **103**, 093001 (2009)] revealed a prominent maximum in the electron energy spectrum very close to the ionization threshold which is not reproduced by widely used Keldysh–Faisal–Reiss (KFR) theories. We have performed fully *ab initio* theoretical analysis and precision calculations to explore the quantum origin of the low energy structure (LES) observed in the experiments. Our study shows that an important role in shaping of LES is played by the effect of Coulomb attraction in the final electron state and the Coulomb threshold effect.

PACS numbers: 32.80.Rm,32.80.Wr

IOP PUBLISHING REVIEW COPY

The phenomenon of above-threshold ionization (ATI) discovered more than 30 year ago [1] and investigations of resulting electron distributions continue attracting much interest [2]. This is related to advances in laser technology which made possible generation of short and intense laser pulses [3]. In particular, tunable long wavelength lasers have become available which allow sufficiently high intensities without saturation of ionization. General properties of the ATI electron energy distributions are well-known. The spectrum consists of a number of peaks separated by the photon energy and corresponding to absorption of a particular number of photons from the laser field. As the energy increases, the spectrum first decreases, then manifests a plateau extending to $10U_p$ [4] ($U_p$ is the ponderomotive potential; for linearly polarized laser fields, $U_p = F^2/(4\omega^2)$ where $F$ is the field strength and $\omega$ is the frequency); formation of the plateau is related to rescattering of the electron in the laser field [5].

Recent experimental observations [6, 7] of above-threshold ionization (ATI) of rare gas atoms and diatomic molecules by mid-infrared laser fields revealed a spike-like maximum in the energy spectra of electrons emitted in the polarization direction of the laser field, in the very vicinity of the ionization threshold. This was called "low-energy structure" (LES) in the ATI spectra. The structure appears a universal ATI feature since it has been detected in all investigated atoms and molecules. What is striking is that LES cannot be described by the widely used quantum mechanical strong-field approximation (SFA) based on the Keldysh–Faisal–Reiss (KFR) theories [8] and thus reveals that current understanding of the intense-field ionization in the long-wavelength regime is incomplete [9]. LES was qualitatively reproduced by numerical solutions of the time-dependent Schrödinger equation of a model system but its physical origin remained unclear [6]. We note that semiclassical models [7], classical trajectory Monte Carlo methods [10], and SFA with Coulomb trajectories [11] were used to simulate ATI at low electron energies. In Ref. [10], emergence of LES was attributed to multiple forward scattering of the ionized electron (a mechanism of laser driven forward Coulomb scattering was proposed earlier by Faisal [9]); in Ref. [11], it was found that low-energy forward scattering leads to caustic structures in semiclassical trajectory calculations which are behind of LES. However, while semiclassical description of LES was given, less attention was paid to the quantum analysis of this phenomenon.

In this paper, we perform a fully quantum mechanical analysis of the ATI spectra of atomic hydrogen and show that the maximum in the energy distribution close to the ionization threshold can be attributed to the quantum effect of Coulomb attraction in the final (continuum) state of the electron. The Coulomb interaction in the final state is neglected in the KFR theories, and that explains their failure in the description of LES.

We start from the expression for the differential ionization probability corresponding to ejection of the electron with the energy $E_\mathrm{f}$ within the unit energy interval and unit solid angle under specified direction (atomic units are used throughout the paper):

$$\frac{\partial^2 P}{\partial E_\mathrm{f} \partial \Omega} = \sqrt{2E_\mathrm{f}}\,|T_\mathrm{fi}|^2\,. \tag{1}$$

The angle-integrated electron energy spectrum can be obtained by integration of Eq. (1) over emission angles:

$$\frac{dP}{dE_\mathrm{f}} = \sqrt{2E_\mathrm{f}} \int d\Omega\ |T_\mathrm{fi}|^2\,. \tag{2}$$

Several alternative expressions can be derived for the transition matrix element $T_\mathrm{fi}$ between the initial and final electron states. We shall use the expression suggested in

* telnov@pcqnt1.phys.spbu.ru
† sichu@ku.edu

Ref. [14]:

$$T_{\rm fi} = -i\int_0^{t_{\rm f}} dt \exp\left(iE_{\rm f}t + \frac{i}{2}\int_0^t \dot{\boldsymbol{b}}^2 d\tau\right)\int d^3r \psi_{\rm f}^*(\boldsymbol{r}-\boldsymbol{b}) \times [U(\boldsymbol{r}) - U(\boldsymbol{r}-\boldsymbol{b})]\exp\left(-i(\dot{\boldsymbol{b}}\cdot\boldsymbol{r})\right)\Psi(\boldsymbol{r},t). \quad (3)$$

Here the time-dependent quantity $\boldsymbol{b}$ has the meaning of the displacement of the "classical" electron under the influence of the laser field only; a dot above $\boldsymbol{b}$ denotes the first derivative with respect to time. The potential $U(\boldsymbol{r})$ represents the interaction with the atomic core; the term $U(\boldsymbol{r})-U(\boldsymbol{r}-\boldsymbol{b})$ decreases at least as $1/r^2$ at large $r$, therefore the spatial integration in Eq. (3) emphasizes the core region of the wave packet. The wave function $\Psi(\boldsymbol{r},t)$ satisfies the time-dependent Schrödinger equation:

$$i\frac{\partial}{\partial t}\Psi(\boldsymbol{r},t) = \left[-\frac{1}{2}\nabla^2 - (\ddot{\boldsymbol{b}}\cdot\boldsymbol{r}) + U(\boldsymbol{r})\right]\Psi(\boldsymbol{r},t). \quad (4)$$

It takes into account the interactions with both the atomic core and laser field (the latter interaction is described in the length gauge, $\ddot{\boldsymbol{b}}$ is the classical acceleration). Before the laser pulse, this function coincides with the initial bound state of the electron.

The final state of the electron $\psi_{\rm f}(\boldsymbol{r})$ describes motion in the atomic field only. As discussed in the scattering theory [15], the correct final states for calculation of the angular distributions are the functions $\psi_{\boldsymbol{k}}^-(\boldsymbol{r})$ which have plane waves and incoming spherical waves asymptotically at large distances. They satisfy the following orthogonality and normalization condition:

$$\langle\psi_{\boldsymbol{k}'}^-(\boldsymbol{r})|\psi_{\boldsymbol{k}}^-(\boldsymbol{r})\rangle = \delta^{(3)}(\boldsymbol{k}-\boldsymbol{k}'). \quad (5)$$

The function $\psi_{\boldsymbol{k}}^-(\boldsymbol{r})$ can be represented as a partial wave expansion:

$$\psi_{\boldsymbol{k}}^-(\boldsymbol{r}) = \frac{1}{(2\pi)^{3/2}}\sum_{l=0}^{\infty}(2l+1)i^l\psi_l^-(k,r)P_l(\cos\vartheta). \quad (6)$$

Here $\psi_l^-(k,r)$ is the radial wave function corresponding to the angular momentum $l$, with proper asymptotic behavior [for a free electron, $\psi_l^-(k,r) = j_l(kr)$ where $j_l(x)$ is the spherical Bessel function]; $\vartheta$ is the angle between $\boldsymbol{k}$ and $\boldsymbol{r}$. Suppose the interaction $U(\boldsymbol{r})$ is short-range. Then for $k\to 0$ and bounded $r$, the radial partial wave $\psi_l^-(k,r)$ can be represented in the following form [15]:

$$\psi_l^-(k,r) = k^l\phi_l(r), \quad (7)$$

where $\phi_l(r)$ depends on $r$ but does not depend on $k$. Thus for small $k$ the main contribution to the final state $\psi_{\boldsymbol{k}}^-(\boldsymbol{r})$ comes from the $s$-wave:

$$\psi_{\boldsymbol{k}}^-(\boldsymbol{r}) \approx \frac{1}{(2\pi)^{3/2}}\phi_0(r) \quad (k\to 0). \quad (8)$$

The situation is quite different for the Coulomb interaction with the atomic core, $U(\boldsymbol{r}) = -Z_c/r$, $Z_c$ being the core charge. The final continuum states $\psi_{\boldsymbol{k}}^-(\boldsymbol{r})$ in the Coulomb field are known in a closed form:

$$\psi_{\boldsymbol{k}}^-(\boldsymbol{r}) = \frac{1}{2\pi}\sqrt{\frac{\nu}{\exp(2\pi\nu)-1}}\exp(i(\boldsymbol{k}\cdot\boldsymbol{r})) \times M(i\nu,1,-i[kr+(\boldsymbol{k}\cdot\boldsymbol{r})]) \quad (9)$$

where $M(a,c,x)$ is the confluent hypergeometric function [16] and $\nu$ is the Coulomb parameter:

$$\nu = -\frac{Z_c}{k}. \quad (10)$$

In the Coulomb case, one arrives at the following result in the limit $k\to 0$:

$$\psi_{\boldsymbol{k}}^-(\boldsymbol{r}) \approx \frac{1}{2\pi}\sqrt{\frac{Z_c}{k}}J_0\left(2\sqrt{2Z_cr}\cos\frac{\vartheta}{2}\right), \quad (11)$$

$J_0(x)$ being the Bessel function. Eq. (11) implies that the probability density of slow electrons in the core region is much higher in the case of Coulomb attraction than in the case of short-range interaction.

Now turn to the expression for the differential ionization probability (1). As one can see, it contains a threshold factor $\sqrt{2E_{\rm f}} = k$ which vanishes at the ionization threshold $E_{\rm f} = 0$. According to Eqs. (3), (6), and (8), for the short-range interaction, the matrix element $T_{\rm fi}$ remains finite as $k\to 0$. Then the probability (1) vanishes at least as $\sqrt{2E_{\rm f}}$ at the ionization threshold. This result can be obtained in the KFR approximation [8] where the Coulomb interaction in the final state is neglected. However, in the case of Coulomb attraction, the matrix element $T_{\rm fi}$ should be calculated with the final state (11). Then the squared absolute value $|T_{\rm fi}|^2$ diverges as $1/k$ for small $k$ and cancels out the threshold factor $\sqrt{2E_{\rm f}}$ in Eq. (1). The differential ionization probability remains finite at $E_{\rm f} = 0$ (in accordance with the Wigner threshold law [12] for Coulomb attraction); in the vicinity of the threshold it is considerably larger than that predicted by the KFR theory. This Coulomb effect can contribute to the emergence of LES observed in the experiments in linearly polarized laser fields [6, 7]. The absence of this structure in circularly polarized fields [6] is also understandable. Multiphoton ionization by circularly polarized laser fields leads to final states with large values of the angular momentum. The centrifugal barrier prevents slow electrons from penetrating the core region; this results in suppression of ionization. Consider the partial wave expansion of the Bessel function in Eq. (11):

$$J_0\left(2\sqrt{2Z_cr}\cos\frac{\vartheta}{2}\right) = \frac{1}{\sqrt{2Z_cr}}\sum_{l=0}^{\infty}(2l+1)(-1)^l \times J_{2l+1}\left(2\sqrt{2Z_cr}\right)P_l(\cos\vartheta). \quad (12)$$

Then the radial wave function corresponding to the angular momentum $l$ appears as follows:

$$\psi_l^-(k,r) = i^l\sqrt{\frac{\pi}{2kr}}J_{2l+1}\left(2\sqrt{2Z_cr}\right). \quad (13)$$

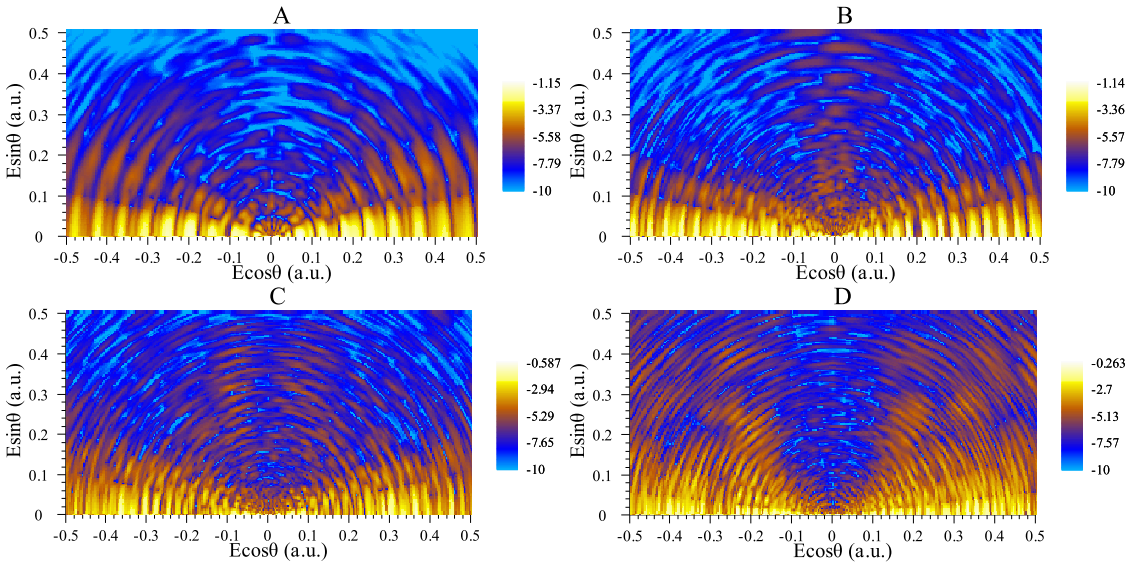


FIG. 1. (Color online) Energy–angle polar surface plots of differential ionization probability; $\theta$ is the ejection angle with respect to the laser field. The duration of the laser pulse is 10 optical cycles, and the peak intensity is $1\times10^{14}$ W/cm$^2$. (A), wavelength 0.8 $\mu$m; (B), wavelength 1.2 $\mu$m; (C), wavelength 1.6 $\mu$m; (D), wavelength 2 $\mu$m.

For $\sqrt{Z_c r} < l$, the Bessel function $J_{2l+1}\left(2\sqrt{2Z_c r}\right)$ can be approximated by the first term of the power series:

$$\psi_l^-(k,r) \approx i^l \sqrt{\frac{\pi Z_c}{k}} \frac{(2Z_c r)^l}{(2l+1)!}. \tag{14}$$

For large $l$, the right-hand side of Eq. (14) is small in the core region, and the corresponding transition amplitude $T_{\rm fi}$ is also small.

To explore LES in the ATI spectra, we have performed *ab initio* calculations for the hydrogen atom subject to linearly polarized mid-infrared laser fields. The laser pulse has a sine-squared envelope, and the classical velocity $\dot{\boldsymbol{b}}$ appears as follows:

$$\dot{\boldsymbol{b}} = \frac{\boldsymbol{F}}{\omega} \sin^2\left(\frac{\omega t}{2N}\right) \sin\omega t. \tag{15}$$

In Eq. (15), $\omega$ is the carrier frequency, $\boldsymbol{F}$ is the peak electric field strength, and $N$ denotes the number of optical cycles in the pulse. In the calculations, we used the laser pulse with 10 optical cycles, the peak field $F$ corresponding to the intensity $1\times10^{14}$ W/cm$^2$ and the carrier wavelengths 0.8 $\mu$m, 1.2 $\mu$m, 1.6 $\mu$m, and 2 $\mu$m (with the Keldysh parameter $\gamma$ values 1.07, 0.71, 0.53, and 0.43, respectively).

The wave functions are computed in the spherical volume with the radius 100 a.u.; we extend the time-dependent generalized pseudospectral (TDGPS) method [13] with 128 radial grid points and 32 angular grid points, allowing *nonuniform* and optimal grid discretization of the spatial coordinates and precision calculation of the time-dependent wave function. Further details of our numerical procedure can be found elsewhere [14].

Fig. 1 shows the differential ionization probabilities (1) as polar surface plots. The radial distance on the plots represents the energy, and the angle points to the direction where the electron is ejected (with respect to the polarization of the laser field). The density (color) corresponds to the differential ionization probability; the density (color) scale is logarithmic. The plots have clear ring structure; the spacing between the rings decreases with the laser wavelength increasing. This behavior is well understood: the rings represent the ATI peaks, and their spacing is equal to the laser frequency (from 1.55 eV at 0.8 $\mu$m to 0.62 eV at 2 $\mu$m). Regarding the angular distributions, one can see that the electrons are mostly ejected in the field direction; however, noticeable side lobes are also present.

Fig. 2 shows the low-energy part of the electron energy spectra in the direction of the laser polarization. The differential ionization probabilities have been averaged with respect to the spatial intensity distribution in the laser focus. The resulting spectra have been also normalized to fall in the range 0 to 1. The solid (blue) lines represent the intensity-averaged quantity $\partial^2 P/(\partial E_{\rm f}\partial\Omega)$ calculated according to Eq. (1) while the dashed (red) lines correspond to the intensity-averaged energy spectra obtained in the Keldysh approximation [8]. In this approximation, the transition matrix element $T_{\rm fi}^{\rm K}$ can be expressed through a 1D time integral since the spatial integration can be performed analytically in the case of the hydrogen atom. For the ionization of the ground state ($E_{\rm i} = -0.5$ a.u.), $T_{\rm fi}^{\rm K}$ reads as

$$T_{\rm fi}^{\rm K} = -\frac{8\sqrt{2}}{\pi} \int_0^{t_{\rm f}} dt \frac{\ddot{\boldsymbol{b}}\cdot(\boldsymbol{k}+\dot{\boldsymbol{b}})}{\left[\left(\boldsymbol{k}+\dot{\boldsymbol{b}}\right)^2 - 2E_{\rm i}\right]^3} \times \exp\left[\frac{i}{2}\int_0^t \left(\boldsymbol{k}+\dot{\boldsymbol{b}}\right)^2 dt' - iE_{\rm i}t\right]. \tag{16}$$

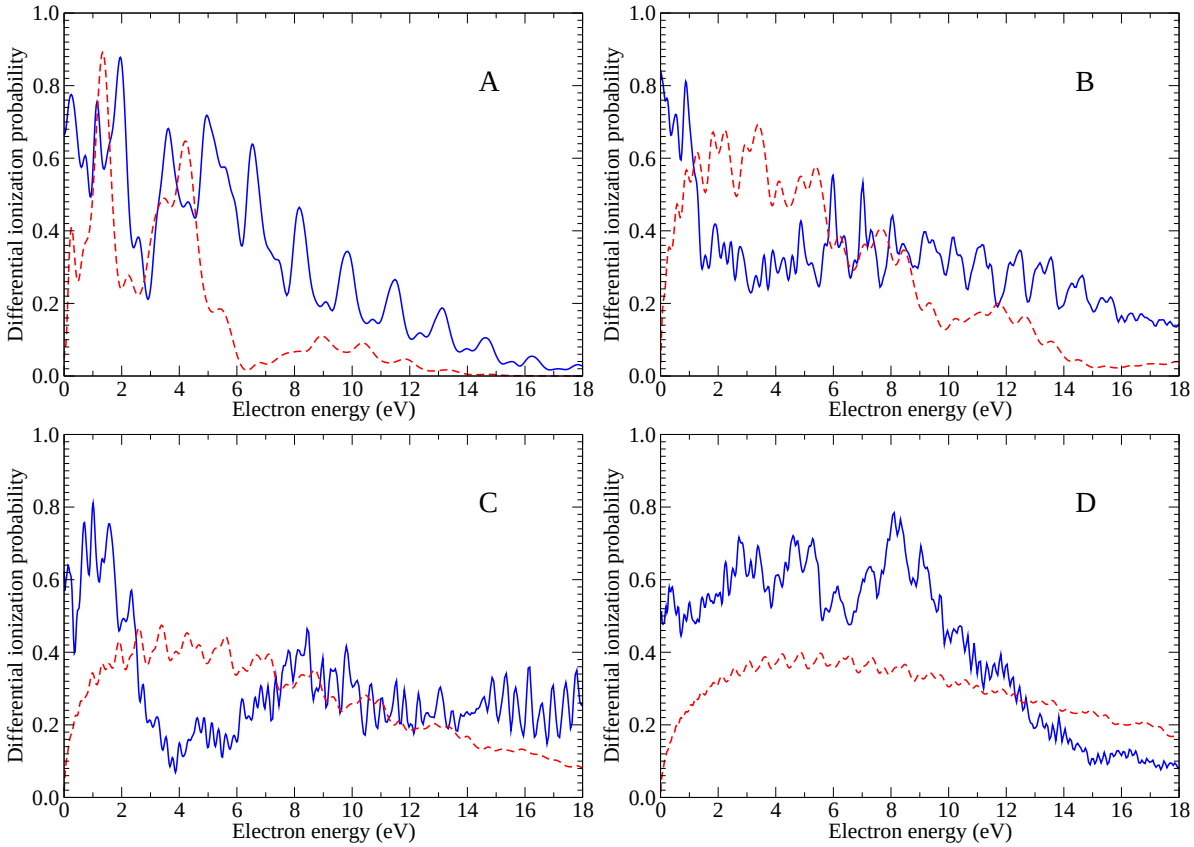


FIG. 2. (Color online) Intensity-averaged energy spectra of the electrons emitted in the polarization direction of the laser field for the 10 optical cycle pulse with the peak intensity $1 \times 10^{14}$ W/cm$^2$. (A), wavelength 0.8 $\mu$m; (B), wavelength 1.2 $\mu$m; (C), wavelength 1.6 $\mu$m; (D), wavelength 2 $\mu$m. Solid (blue) line shows the energy spectrum computed according to Eqs. (1), (3) while dashed (red) line corresponds to the Keldysh approximation (Eqs. (1), (16)).

Since the positions of individual ATI peaks in the energy spectrum depend linearly on the ponderomotive potential $U_p$, the intensity average is expected to wash out the ATI peak structure of the spectrum in the case of low-frequency fields ($U_p \gg \omega$, the shift of the peaks when the intensity is varied in the laser focus is much larger than the spacing between the peaks). As one can see from Fig. 2, this is the case for the wavelengths 2 $\mu$m and (to some extent) 1.6 $\mu$m while at 1.2 $\mu$m and, particularly, at 0.8 $\mu$m distinct ATI peaks are still present. In the latter case, the large separation between the ATI peaks (1.55 eV), comparable to the width of LES itself, prevents from shaping a wider maximum which can be seen at larger wavelengths. It is instructive to compare the behavior of the exact and Keldysh electron energy spectra in the vicinity of the ionization threshold. At 0.8 $\mu$m (Fig. 2A), there is no qualitative difference except for the energies below 1 eV: in the energy range 1 to 5 eV both spectra show similar ATI peaks. At larger wavelengths, however, the Keldysh spectra exhibit a clear signature of the $\sqrt{2E_\mathrm{f}}$ threshold factor. The larger the wavelength, the longer the energy interval near the threshold where this factor dominates the spectrum. As a result, the Keldysh electron energy spectra are suppressed in the vicinity of the ionization threshold. In contrast, the exact spectra are not suppressed and have a prominent maximum in the vicinity of the threshold, in accordance with the experimental observations [6, 7].

To investigate the role of the attractive Coulomb interaction in the final state in the emergence of this maximum, we have performed another calculation of the electron energy spectra in the polarization direction, with the transition matrix element $T^0_\mathrm{fi}$ computed according to Eq. (3) but using the unperturbed ground-state wave function $\psi_{1s}(\boldsymbol{r})\exp(-iE_\mathrm{i}t)$ under the integral instead of the exact one:

$$T^0_\mathrm{fi} = -i\int_0^{t_\mathrm{f}} dt \exp\left(i(E_\mathrm{f}-E_\mathrm{i})t + \frac{i}{2}\int_0^t \dot{\boldsymbol{b}}^2 d\tau\right) \times \int d^3r \psi^*_\mathrm{f}(\boldsymbol{r}-\boldsymbol{b})[U(\boldsymbol{r})-U(\boldsymbol{r}-\boldsymbol{b})]\psi_{1s}(\boldsymbol{r}) \times \exp\left(-i(\dot{\boldsymbol{b}}\cdot\boldsymbol{r})\right). \quad (17)$$

In this approximation, the final state Coulomb interaction is still taken into account while possible excitations of intermediate bound states and rescattering effects are missing. The results are presented in Fig. 3; again, all the spectra are intensity-averaged and normalized. As

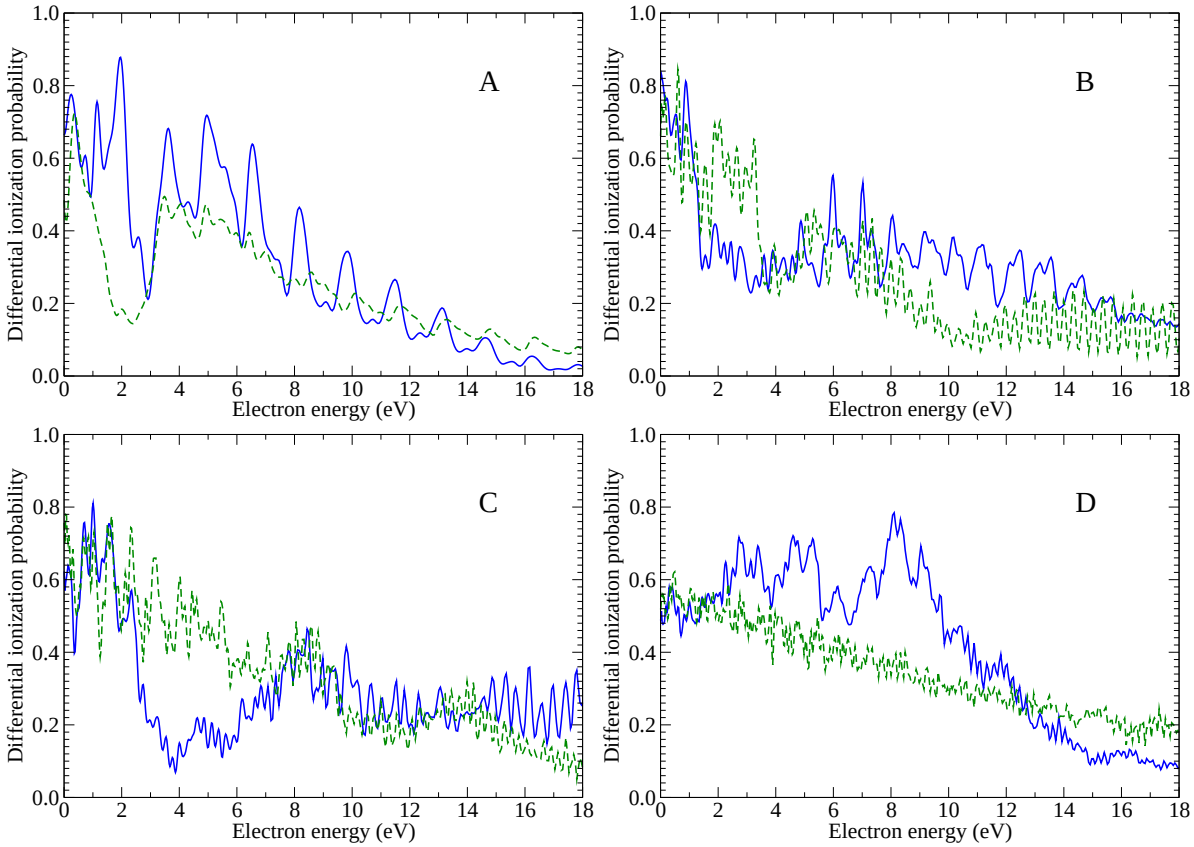


FIG. 3. (Color online) Intensity-averaged energy spectra of the electrons emitted in the polarization direction of the laser field for the 10 optical cycle pulse with the peak intensity $1 \times 10^{14}$ W/cm$^2$. (A), wavelength 0.8 $\mu$m; (B), wavelength 1.2 $\mu$m; (C), wavelength 1.6 $\mu$m; (D), wavelength 2 $\mu$m. Solid (blue) line shows the exact energy spectrum computed according to Eqs. (1), (3) while dashed (green) line corresponds to an approximation where the exact time-dependent wave function in Eq. (3) is replaced by the unperturbed ground state wave function.

one can see, compared with the KFR theory, the current approximation gives fairly good results near the threshold (at the electron energies 0 to 2 eV, where the LES peak is expected [6] for the laser wavelengths and intensity used in our calculations). For the wavelengths 1.2 $\mu$m and longer, discrepancies with the exact energy spectra appear significant for the energies larger than 2 eV. We may conclude that the proper account of the Coulomb interaction in the final state is crucial for the correct description of the electron energy spectra in the very vicinity of the ionization threshold (0–2 eV). Other effects such as rescattering of ejected electrons may be important at larger energies. The large peaks seen at the wavelength 2 $\mu$m in the energy interval 4 to 10 eV are not directly related to LES. They may appear due to enhancement of the second maximum in the electron spectra also observed at the wavelengths 1.2 $\mu$m and 1.6 $\mu$m approximately at the same energy.

In summary, we have performed a quantum mechanical analysis of the multiphoton ionization amplitude in the vicinity of the threshold. We have shown that the exact amplitude, in contrast with the KFR approximation, does not vanish at the threshold provided the interaction of the ejected electron with the residual is represented by the attractive Coulomb potential. In the attractive Coulomb field, the density of slow electrons is condensed in the core region favoring the ionization process. We have performed numerical calculations on the hydrogen atom subject to intense mid-infrared laser fields with the wavelengths 0.8 $\mu$m to 2 $\mu$m. In accordance with the theoretical predictions, the numerical data show a maximum close to the threshold in the energy spectra of the electrons emitted in the polarization direction of the laser field, similar to the low-energy structure revealed by recent experiments on noble gas atoms and diatomic molecules. While the Coulomb threshold effect alone may not explain the whole picture of the low-energy ATI electron spectra, it plays an important role in shaping of such spectra, including emergence of LES.

This work was partially supported by the Chemical Sciences, Geosciences and Biosciences Division of the Office of Basic Energy Sciences, Office of Sciences, U. S. Department of Energy, and by the U. S. National Science Foundation. We also acknowledge the partial support of National Science Council of Taiwan (Grant No. 97-2112-M-002-003-MY3) and National Taiwan University

(Grants No. 98R0045 and 99R80870).


[1] P. Agostini *et al.*, Phys. Rev. Lett. **42**, 1127 (1979).
[2] W. Becker *et al.*, Adv. At. Mol. Opt. Phys. **48**, 35 (2002).
[3] F. Krausz and M. Ivanov, Rev. Mod. Phys. **81**, 163 (2009).
[4] G. G. Paulus, W. Becker, W. Nicklich, and H. Walther, J. Phys. B **27**, L703 (1994); M. Lewenstein, K. C. Kulander, K. J. Schafer, and P. H. Bucksbaum, Phys. Rev. A **51**, 1495 (1995); J. Z. Kamiński, A. Jaroń, and F. Ehlotzky, Phys. Rev. A **53**, 1756 (1996).
[5] P. B. Corkum, Phys. Rev. Lett. **71**, 1994 (1993); J. L. Krause, K. J. Schafer, and K. C. Kulander, Phys. Rev. Lett. **68**, 3535 (1992).
[6] C. I. Blaga *et al.*, Nature Phys. **5**, 335 (2009).
[7] W. Quan *et al.*, Phys. Rev. Lett. **103**, 093001 (2009).
[8] L. V. Keldysh, Zh. Eksp. Teor. Fiz. **47**, 1945 (1964) [Sov. Phys. JETP **20**, 1307 (1965)]; F. H. M. Faisal, J. Phys. B **6**, L89 (1973); H. R. Reiss, Phys. Rev. A **22**, 1786 (1980).
[9] F. H. M. Faisal, Nature Phys. **5**, 319 (2009).
[10] C. Liu and K. Z. Hatsagortsyan, Phys. Rev. Lett. **105**, 113003 (2010).
[11] T. M. Yan, S. V. Popruzhenko, M. J. J. Vrakking, and D. Bauer, Phys. Rev. Lett. **105**, 253002 (2010).
[12] E. P. Wigner, Phys. Rev. **73**, 1002 (1948).
[13] X. M. Tong and S. I. Chu, Chem. Phys. **217**, 119 (1997).
[14] D. A. Telnov and S. I. Chu, Phys. Rev. A **79**, 043421 (2009).
[15] R. G. Newton, *Scattering theory of waves and particles*, (McGraw-Hill, New York, 1966).
[16] M. Abramowitz and I. Stegun (Eds.), *Handbook of Mathematical Functions*, (Dover, New York, 1965).